Effects of Lattice Defect Types in Cuo Absorber Layer on the Solar Cell Performance

Galsan.T. Kamal[1], Nadim.K. Hassan[2], Abdulrahman Rashid Hammood[3], Abdul Kareem Dahash Ali[4]

[1]Department of physics, College of Education for pure science, University of Tikrit, abdulrahmman002@gmail.com
[2]Department of physics, College of Education for pure science, University of Tikrit.
[3]Department of Vocational Education, Anbar Education Directorate.
[4]Department of physics, College of Education for pure science, University of Tikrit.

This study investigates the structural composition and performance optimization of an ultra-thin solar cell employing a layered architecture consisting of Al/TiO2/CdS/CuO/Au/glass. The TiO2 layer serves as the window layer with a wide energy gap of approximately 3.2 eV, followed by the CdS buffer layer with an energy gap of 2.4 eV, facilitating alignment between the window and absorption layers. The p-type CuO absorption layer, with an energy gap ranging from 1.21 to 1.51 eV, functions as the primary absorber. Numerical simulations conducted using SCAPS-1D software provide insights into the electrical characteristics and performance optimization of the solar cell. Results demonstrate that varying the thickness of the CuO absorption layer and the density of bulk defects significantly impact electrical properties, with an optimal thickness of 2 µm identified. Additionally, reducing the thickness of the CdS layer enhances conversion efficiency, fill factor, open circuit voltage, and short circuit current due to increased carrier penetration into the absorption layer, particularly for shorter wavelengths. Furthermore, the interplay between bulk and interface defects influences electrical parameters, with interface defects exerting a more pronounced effect on quantum efficiency. These findings offer valuable insights into enhancing the design and performance of solar cells through structural optimization and defect management strategies.

Keywords: CuO, TiO2 , CdS ,solar cell , Numerical simulation , SCAPS-1D ,defects, interface defects.

1. Introduction

Semiconductors are essential components across a broad spectrum of applications, spanning from photovoltaic systems to optoelectronics and beyond. Their significance is evident in the operation of photovoltaic (PV) systems [1], thermoelectric (TE) devices [2], batteries [3-5], transistors [6, 7], photonic devices [8], and phase-change memory devices [9]. As the global demand for renewable energy escalates, research efforts are increasingly directed towards

advancing production methods and identifying cost-effective materials for solar cells, which stand as pivotal solutions for sustainable energy solutions. While silicon-based solar cells have historically dominated the market, recent years have witnessed a burgeoning interest in alternative materials, spurred by the urgent need for environmental sustainability.

In this context, titanium dioxide (TiO_2) and copper oxide (CuO) have emerged as promising candidates poised to revolutionize solar cell technology. However, despite its potential, the efficacy of TiO_2 as a primary material in solar cells remains a subject of active investigation. Researchers have recently been working to improve the performance and efficiency of TiO_2-based solar cells by coming up with new ways to synthesize materials, designing smart interfaces, and testing out new device architectures.

Moreover, the exploration of TiO_2 and CuO heterojunctions represents a frontier in both photocatalytic applications and solar cell development. Notably, recent studies have demonstrated the significant potential of these heterojunctions in enhancing the efficiency and stability of solar energy conversion devices. P-type semiconductor materials such as Cu_2O or CuO, deployed as absorber layers, boast narrow direct band gaps, rendering them well-suited for solar energy harvesting. Additionally, TiO_2, characterized by a wide bandgap exceeding 3 eV, exhibits versatility across various applications, including dye-sensitized solar cells.

Despite these strides, challenges persist in fully unlocking the potential of TiO2-based solar cells. Mitigating issues such as charge carrier recombination, optimizing interface engineering, and ensuring device scalability remain critical imperatives in harnessing the transformative capabilities of TiO_2 and CuO in solar energy conversion. Researchers are working on making TiO_2/CuO-based solar cells commercially viable and widely used by using cutting-edge materials science, new device engineering, and complex theoretical modeling. They hope that this will pave the way for a sustainable energy future. The goal of this study is to contribute to understanding and improving the performance of Al/TiO_2/CdS/CuO/Au/glass-based solar cells through theoretical and experimental research.

2. Methodology

2.1 Solar cell design:

The architecture of solar cells is of capital importance because it must reconcile several essential parameters, such as simplicity, performance, and the affordable cost necessary for their realization. In this context, the system proposed and studied in this document integrates all these considerations by adopting a structure composed of several layers arranged in a specific order: Al/TiO_2/CdS/CuO/Au/glass, illustrated in Figure 1. At the heart of this innovative design, titanium dioxide (TiO_2) assumes a central role as a window layer, renowned for its exceptional transparency and imposing energy band gap of approximately 3.2 eV. This fundamental layer constitutes a key element to guarantee optimal light absorption and efficient electronic excitation within the solar cell.

Subsequently, the buffer layer, composed of cadmium sulfide (CdS), is strategically positioned to ensure a smooth transition between the window and absorption layers. Featuring an energy bandgap of 2.4 eV, CdS plays a crucial role as a critical interface layer in this structure, facilitating the efficient transport of electrons across the cellular structure.

At the heart of the solar cell lies the p-type absorption layer, made of CuO, proposed in this architecture to maximize light absorption and the generation of electron-hole pairs. With an energy band gap varying from 1.21 to 1.51 eV, CuO can play a fundamental role in harnessing solar energy and triggering the photovoltaic process. The proposed design of this solar cell emphasizes simplicity and accessibility, thereby providing a pathway for efficient manufacturing through a multitude of affordable techniques. From spin coating to sol-gel deposition, magnetron sputtering, and thermal deposition. This versatility in manufacturing techniques not only helps improve production scalability of this proposed structure but also paves the way for widespread adoption and integration of this architecture into various applications, thereby contributing to the global transition to sustainable energy solutions.

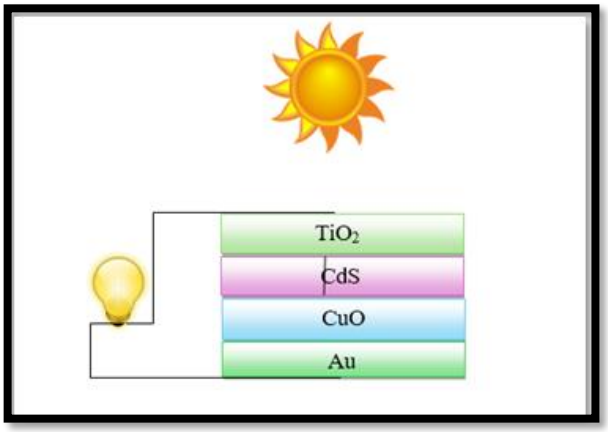

Figure 1: a schematic view diagram of the optimized ultra-thin Al/TiO_2/CdS/CuO/Au/glass solar cell.

2.2 Numerical simulation:

To optimize the performance of the ultra-thin Al/TiO_2/CdS/CuO/Au/glass solar cell, we employ a numerical simulation conducted through SCAPS-1D, an innovative one-dimensional solar cell modeling program developed at the Department of Electronics and Information Systems (EIS), University of Gent. This software represents the forefront of precision and innovation in solar cell research, providing a sophisticated platform for simulating and refining solar cell designs. Crafted with meticulous attention to detail, SCAPS-1D serves as an indispensable tool for researchers and engineers, enabling in-depth analysis of solar cell performance and characteristics. Its versatile capabilities encompass the accommodation of intricate cell architectures, including those with multiple layers and complex material compositions. With its intuitive interface and robust computational algorithms, SCAPS-1D empowers users to explore a diverse array of parameters, ranging from material properties to device geometries, thereby facilitating the optimization of solar cell efficiency and overall performance. The software fundamentally relies on the rigorous solution of semiconductor equations, starting with the formulation of fundamental equations like the Poisson equation.

$$-\frac{d^2\psi}{dx^2} = \frac{dE}{dx} = \frac{q}{\varepsilon_s}[p + n + N_D^+ - N_A^-] \quad [1]$$

Where N_D represents the concentration of donors and N_A represents the concentration of acceptors. ψ represents the electrostatic potential, E stands for the electric field, P denotes the hole density, n signifies the electron density, and ε_s represents the relative permittivity.

The following relationship results in the continuity equation.

$$\frac{\partial n}{\partial t} = \frac{1}{q}\frac{\partial J_n}{\partial x} + G_n - R_n \qquad [2]$$

$$\frac{\partial p}{\partial t} = -\frac{1}{q}\frac{\partial J_p}{\partial x} + G_p - R_p \qquad [3]$$

Where G_p represents the rate of electron-hole creation, R is the rate of electron-hole recombination, and Jn (J_p) is the current density of electron-hole pairs. The equations for diffusion and drift density of charge carriers are derived by solving the Poisson and continuity equations.. [22].

$$Jn = q(n\mu_n E + Dn\frac{dn}{dx}) \qquad [4]$$

$$Jp = q(n\mu_p E + Dp\frac{dp}{dx}) \qquad [5]$$

Where q The charge , μn (μp) are the mobility of electron (hole) , (E)electric field, (D) diffusion coefficient .

The solar cell's total current was determined using the following equation [23]:

$$I = I_0\left(\exp\frac{qV}{nKT} - 1\right) - I_L \qquad [6]$$

Here, T represents the temperature in Kelvin, K stands for the Boltzmann constant, and IL denotes the light current. The computation of the open circuit voltage (V_{OC}), which attains its peak value when the current is zero, relies on the subsequent equation:

$$V_{OC} = \frac{KT}{q}\,\mathrm{Ln}\left(\frac{I_L}{I_o} - 1\right) \approx \frac{KT}{q}\,\mathrm{Ln}\left(\frac{I_L}{I_o}\right) \qquad [7]$$

Where I_0 signifies the saturation current, derivable using the formula:

$$I_0 = A\left[\frac{q\,D_n n_i^2}{L_n N_A} + \frac{q\,D_p n_i^2}{L_p N_D}\right] \qquad [8]$$

The dimensions of the diode's cross-sectional area, represented by Ln and Lp, correspond respectively to the electron and hole diffusion lengths. The correlation between short circuit current (I_{SC}) and open circuit voltage (V_{OC}) is articulated as:

$$Isc = I_0\left(\exp\frac{qvoc}{kT} - 1\right) \qquad [9]$$

Where, Voc, Isc, η, FF are variables interconnected through the following equations [21].

$$FF = \frac{V_{max}\,I_{max}}{V_{oc}\,I_{sc}} \qquad [10]$$

$$\eta = \frac{Pmax}{p_{in}} \times 100\%. \qquad [11]$$

$$where \quad P_{max} = VocISCFF \qquad [12]$$

$$\eta = \frac{FF \times I_{sc} \times V_{oc}}{p_{in}} \times 100\% \quad [13]$$

Determining the minority carrier lifetime is paramount as it signifies the average duration for minority carriers to recombine. This crucial parameter is intricately linked to the concentrations of doping and recombination and adheres to a specific relationship [24]:

$$\tau = \frac{1}{\sigma V_{th} N_t} \quad [14]$$

$$\tau = \frac{\Delta n}{R} \quad [15]$$

Here, R represents the recombination rate, σ denotes the capture cross-section, Nt stands for the defect concentration, Vth represents the thermal speed, and Δn indicates the excess minority carrier concentration.

The efficiency of a solar cell can be significantly impacted by the mobility of charge carriers within the bulk semiconductor material [25]. Mobility plays a critical role in determining the minority carrier diffusion length (L_{diff}), which represents the distance a carrier can travel within a semiconductor before recombining. Equation 16 outlines the definition of the minority carrier diffusion length [26]:

$$L_{diff} = \sqrt{D\,\tau} \quad [16]$$

Here, D represents the diffusion coefficient, and τ denotes the minority carrier lifetime. Equation 17 elucidates the relationship for the diffusion coefficient:

$$D = \mu \frac{KT}{q}$$

In this equation, μ signifies the carrier mobility, (q) denotes the charge of the carrier, k stands for Boltzmann's constant, and (T) represents the temperature. [17]

Equation 18 will be the result of substituting the value of equation 17 for equation 16 in that order.

$$L_{diff} = \sqrt{\mu \frac{KT}{q} \tau} \quad [18]$$

Equation 18 states that the diffusion length is greatly influenced by the mobility of minority carriers. Enhanced mobility leads to a higher probability of photogenerated charge carriers gathering at the terminals, which enhances photocurrent in a solar cell. A reduction in mobility leads to decreased efficiency of solar cells.

3. Results and discussion

3.1 Impact of Absorption Layer Thickness and Density of Bulk Defects:

In this study, we investigated the influence of varying the thickness and density of defects within the absorption layer (CuO) on the performance of the solar cell. The thickness of the CuO layer was systematically adjusted within the range of 0.5 to 2.5 µm, while simultaneously altering the defect density within the range of 10^{13} to 10^{16} cm^{-3} at each thickness, following a Gaussian distribution. It's worth noting that the parameters for the

other layers, such as compatibility and penetration, remained constant throughout the experiments. The introduced defects were predominantly of the donor type, positioned 0.6 eV away from the valence band.

Figure (2) illustrates the observed trends as the thickness of the absorption layer is increased. A noticeable enhancement in the electrical properties, including V_{OC}, J_{SC}, fill factor (F.F), and overall efficiency (η), is evident. This improvement can be attributed to the increased absorption coefficient resulting from the thicker absorption layer. As the thickness increases, the absorption of incident light within the absorption layer also increases, leading to a more efficient utilization of photons and consequently improved electrical characteristics of the solar cell.

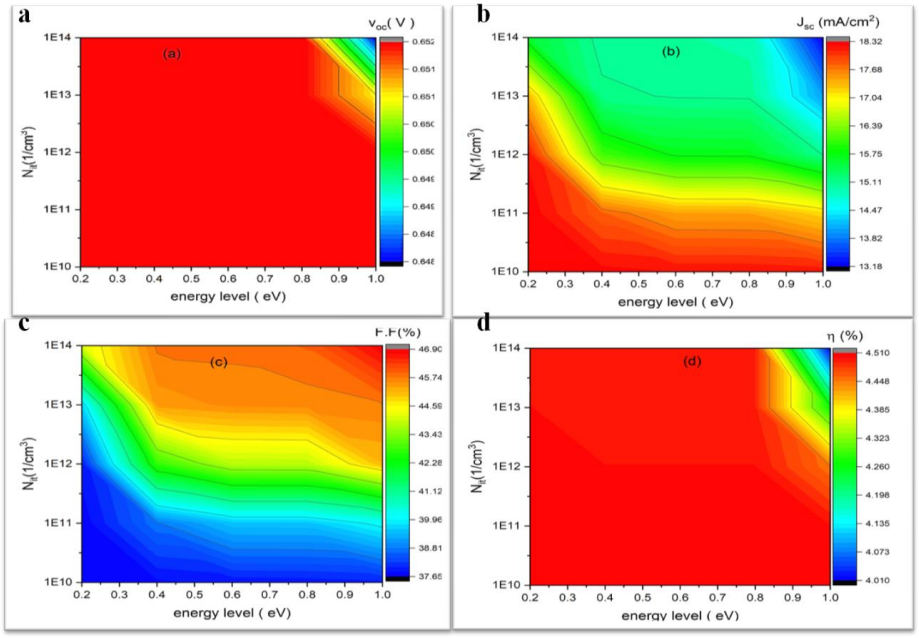

Fig. 2: (a), (b), (c), and (d) depict the impact of absorber layer thickness and defect density on the parameters V_{OC}, J_{SC}, FF, and η of the Al/TiO_2/CdS/CuO/Au/glass solar cell, respectively.

A noteworthy variation in electrical characteristics was observed in response to changes in thickness, particularly when the density of defects was below 10^{14} cm^{-3}, suggesting a discernible influence of thickness on performance. However, this influence becomes negligible when the defect density surpasses 10^{14} cm^{-3}, indicating that the effect of defect density outweighs that of thickness. As depicted in Figure (3a), when defect density exceeds $10^{14}cm^{-3}$, the impact of thickness diminishes due to increased carrier recombination. Notably, the optimal thickness of the absorption layer was found to be 2 µm.

Further analysis from Figure (3) revealed that the performance of the solar cell remains relatively unaffected when the defect density is below 10^{14} cm^{-3}. However, a substantial deterioration in electrical properties was observed when the defect density exceeded $10^{14}cm^{-3}$. This decline can be attributed to the increased recombination of carriers due to the

heightened concentration of defects, acting as capture centers for carriers, as illustrated in Figure (3b). Consequently, this led to a significant degradation in fill factor (FF), efficiency (η), short-circuit current (J_{SC}), and open-circuit voltage (V_{OC}) as the defect concentration increased.

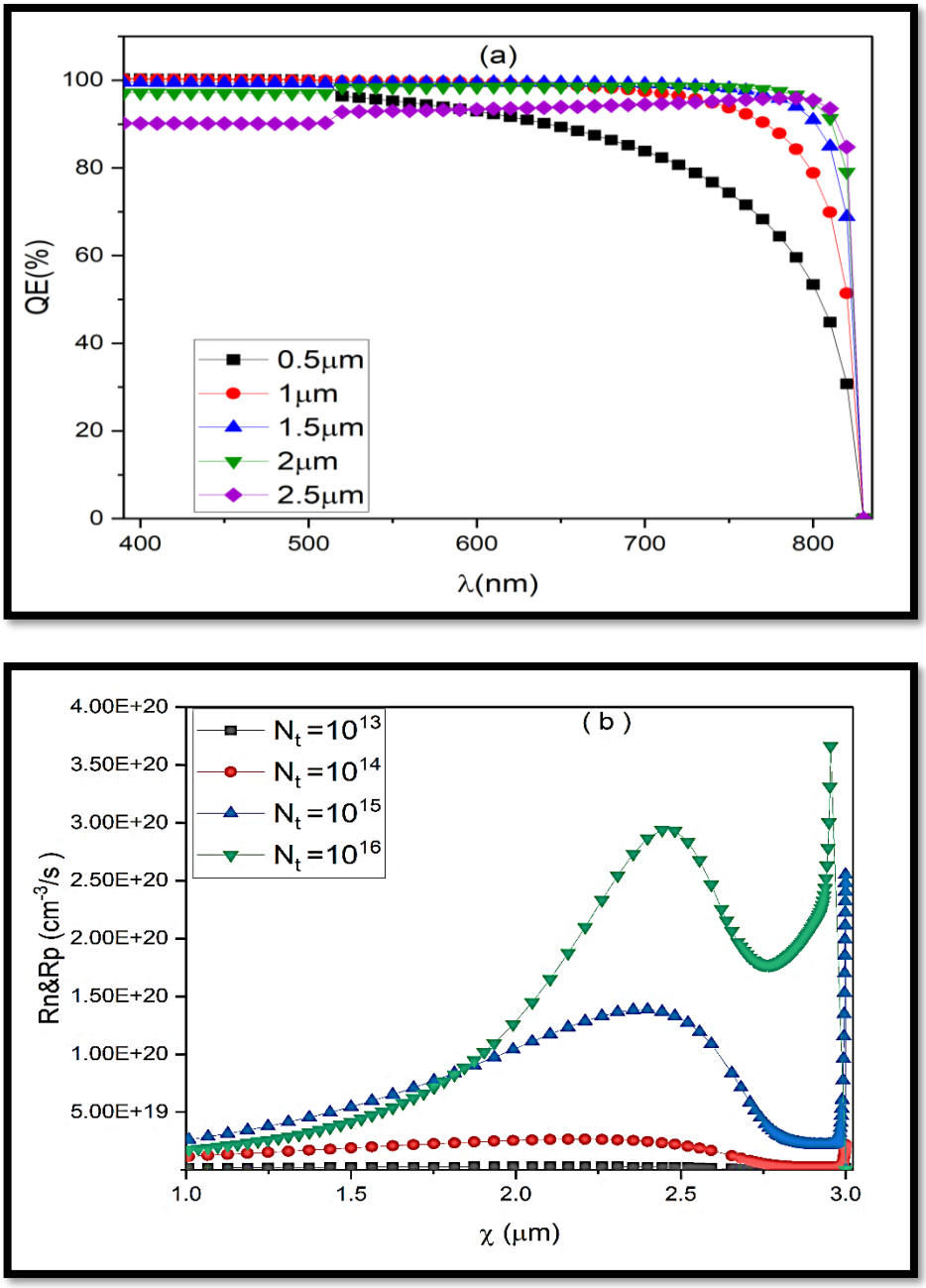

Fig. 3: (a) Quantum efficiency with change in absorption layer thickness (b) Recombination

of carriers with change in defect concentration

3.2 Exploring the impact of CdS layer thickness amidst bulk defects:

Examining the influence of CdS layer thickness while maintaining bulk defects at a constant density of 10^{16} $cm^{-3}$and holding all other parameters steady reveals intriguing insights, as depicted in Figure (4). Notably, a reduction in CdS layer thickness correlates with notable enhancements in conversion efficiency, fill factor, open-circuit voltage, and short-circuit current. This phenomenon can be attributed to the increased percentage of carriers traversing into the absorption layer as the CdS layer thickness decreases. Consequently, this escalation facilitates a higher absorption of photons with energies surpassing the absorption layer's energy gap. This heightened absorption efficiency, particularly for photons with energies exceeding the absorption layer's band gap, translates into improved electrical characteristics of the solar cell.

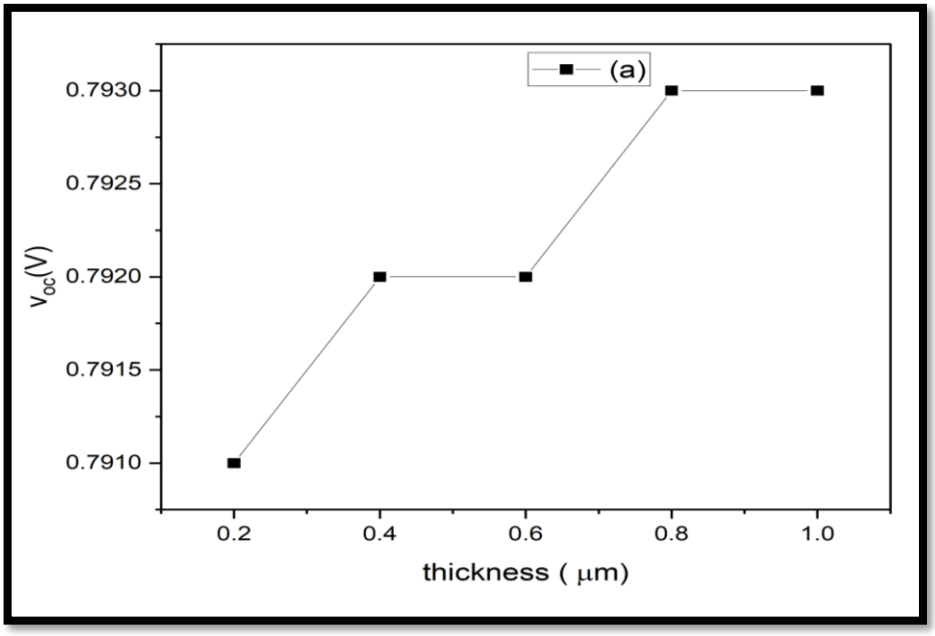

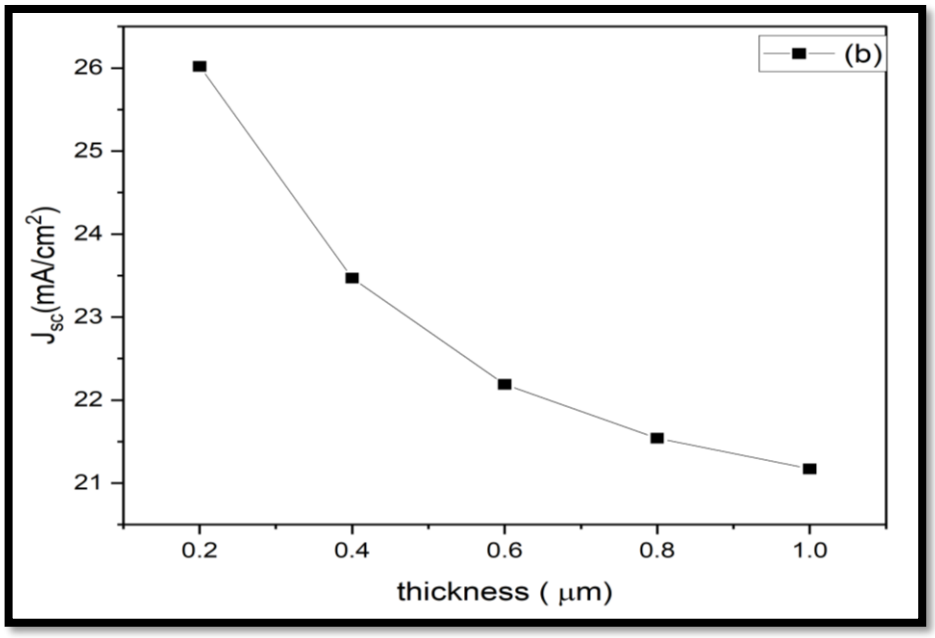
(b)
J_{sc}(mA/cm^2)
26
25
24
23
22
21
0.2
0.4
0.6
0.8
1.0
thickness (μm)

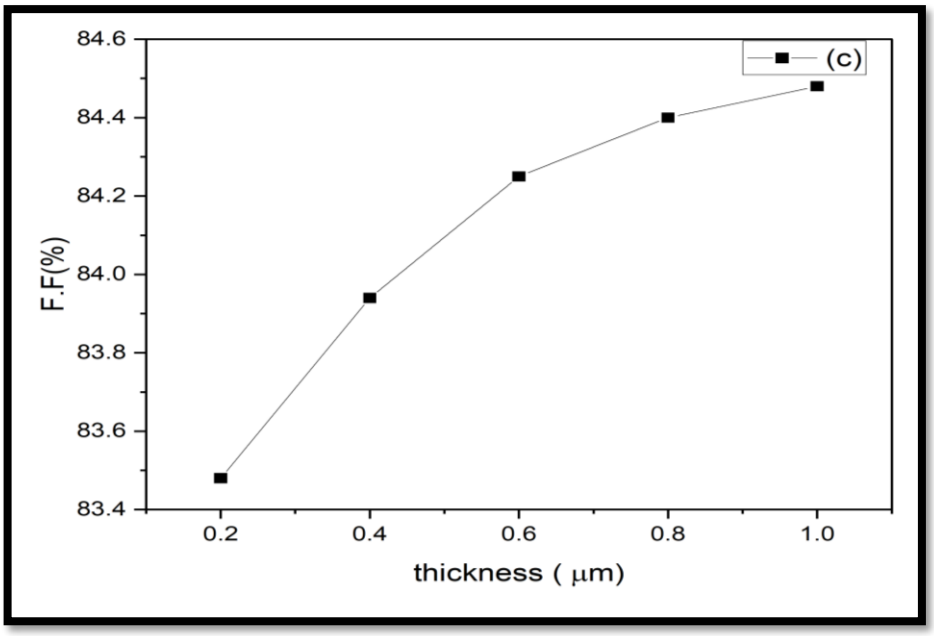
(c)
F.F(%)
84.6
84.4
84.2
84.0
83.8
83.6
83.4
0.2
0.4
0.6
0.8
1.0
thickness (μm)

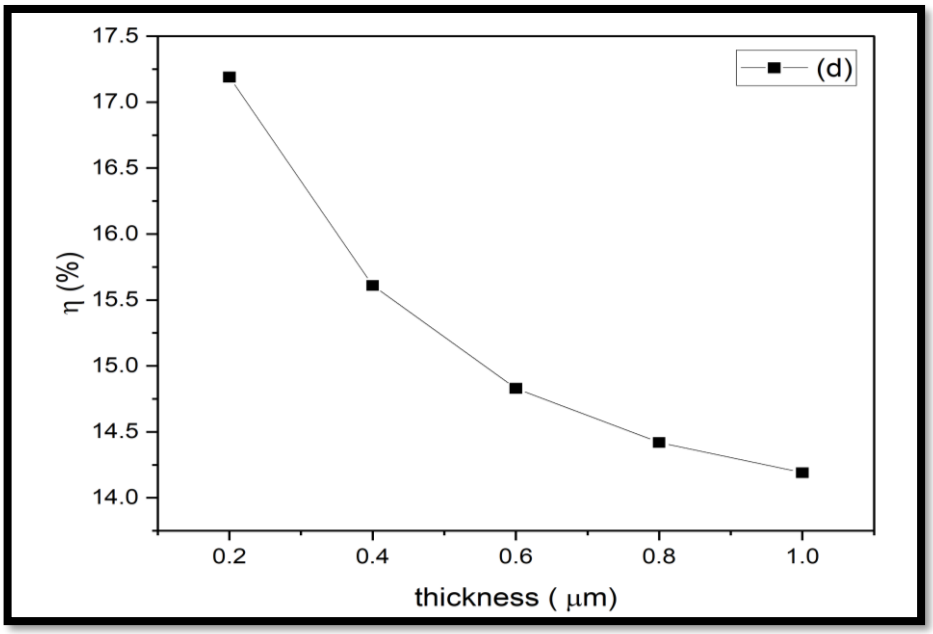

Fig. (4) The effect of the thickness of the buffer layer on the (a) voc (b) jsc (c) F.F (d) eta of the solar cell with bulk defects.

Further analysis, as illustrated in Figure (5), highlights the significant influence of CdS layer thickness primarily in the domain of short wavelengths. Intriguingly, the optimal CdS layer thickness was identified to be 0.2 μm, yielding superior cell performance across various output metrics. This optimal thickness underscores the delicate balance necessary for effective photon absorption and carrier transport within the solar cell structure, ultimately culminating in optimized device performance.

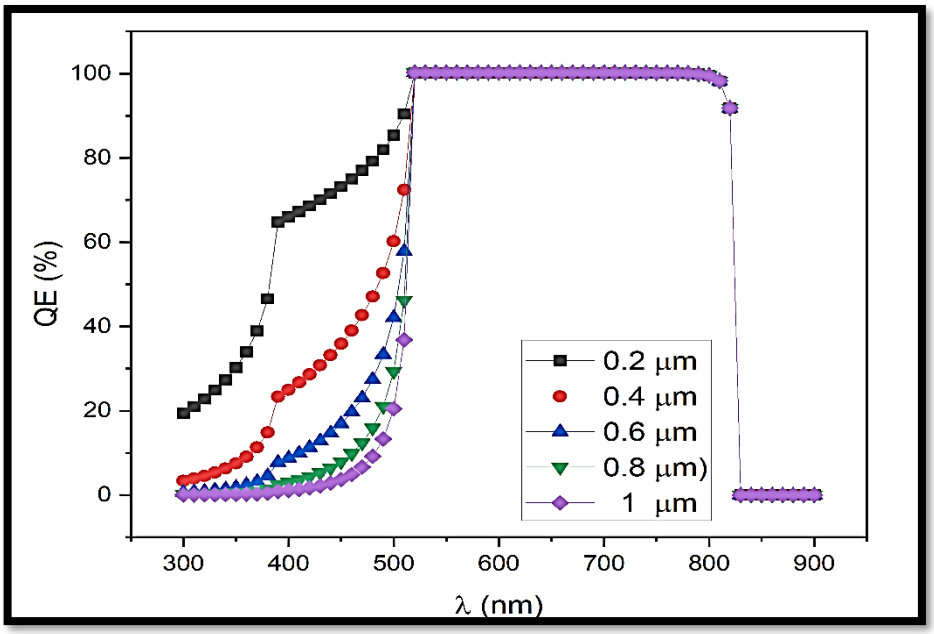

Fig. (5) Quantitative efficiency with changing the buffer layer thickness

3.3 Exploring the Impact of Bulk and Interface Defects on Solar Cell Performance

In our investigation into the effects of bulk and interface defects on solar cell operation, Figure (6) illustrates variations in defect densities within the matrix ranging from 10^{13} to 10^{16} cm^{-3}, alongside interface defect densities spanning 10^{10} to 10^{14} cm^{-2}. The results unveil intriguing nuances in V_{OC}, J_{SC}, fill factor (FF), and overall efficiency (η) in response to these variations. Notably, at a fixed interface defect density of 10^{10} cm^{-2}, altering the bulk defect density from 10^{13} to 10^{16} cm^{-3} induces slight changes in Voc, Jsc, FF, and η. For instance, when the bulk defect density is fixed at 10^{16} cm^{-3}, V_{OC} transitions from 0.796 to 0.666 V, Jsc decreases from 27.61 to 22.59 mA/cm^2, FF declines from 80.6 to 41.37 %, and η diminishes from 17.59% to 6.23%.

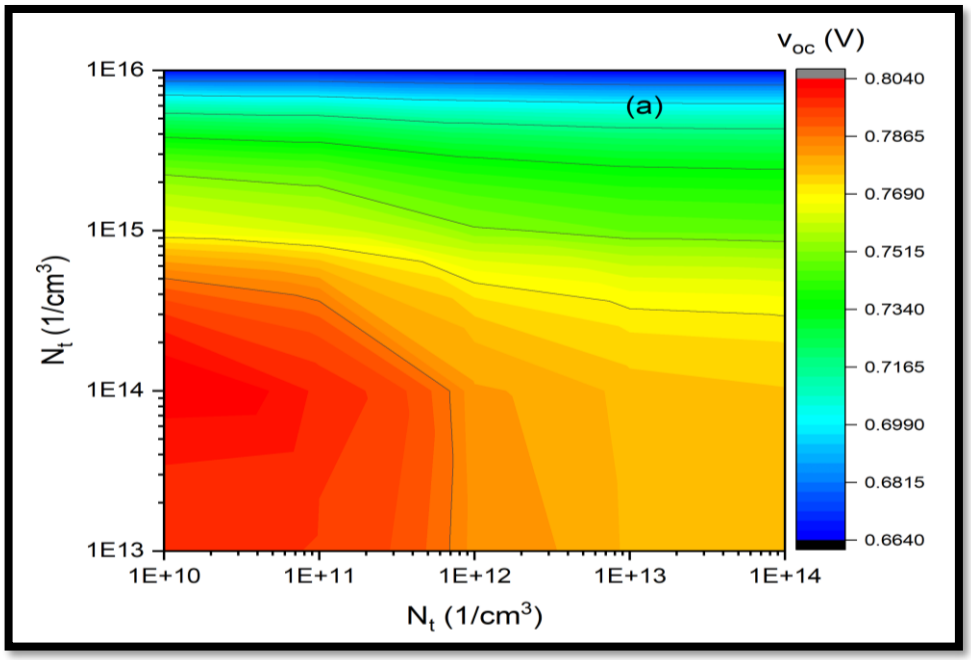
v_{oc} (V)
0.8040
0.7865
0.7690
0.7515
0.7340
0.7165
0.6990
0.6815
0.6640
(a)
1E16
1E15
1E14
1E13
N_t (1/cm^3)
1E+10
1E+11
1E+12
1E+13
1E+14
N_t (1/cm^3)

(a)

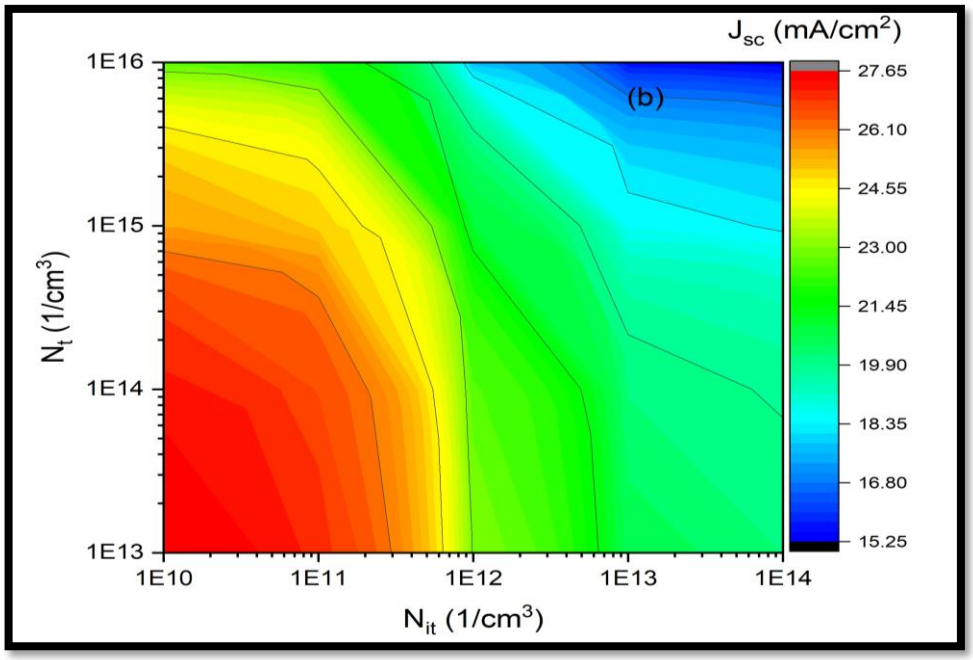
J_{sc} (mA/cm^2)
27.65
26.10
24.55
23.00
21.45
19.90
18.35
16.80
15.25
(b)
1E16
1E15
1E14
1E13
N_t (1/cm^3)
1E10
1E11
1E12
1E13
1E14
N_{it} (1/cm^3)

(b)

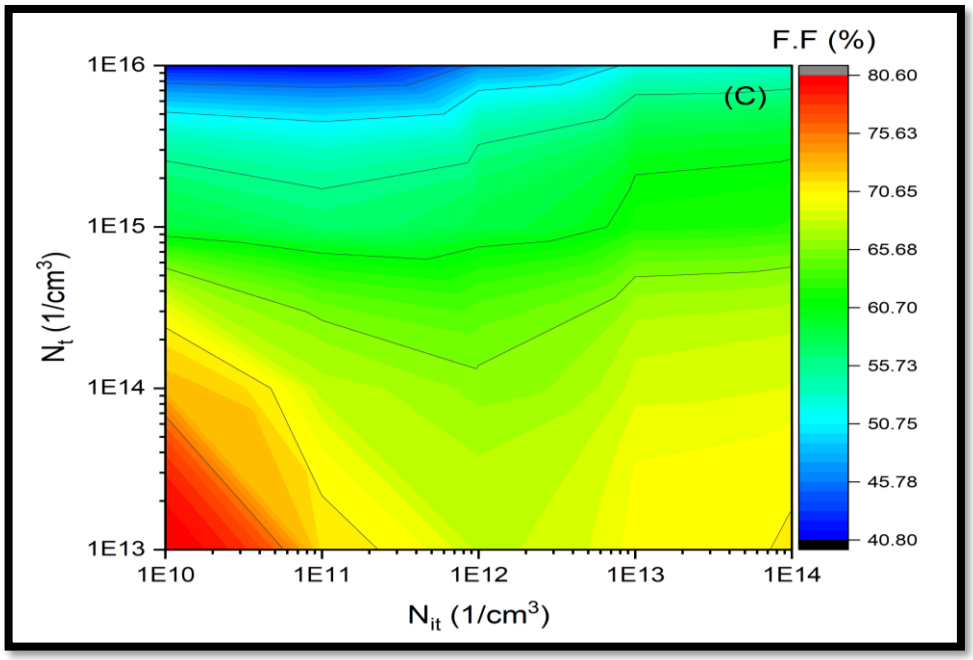

(c)

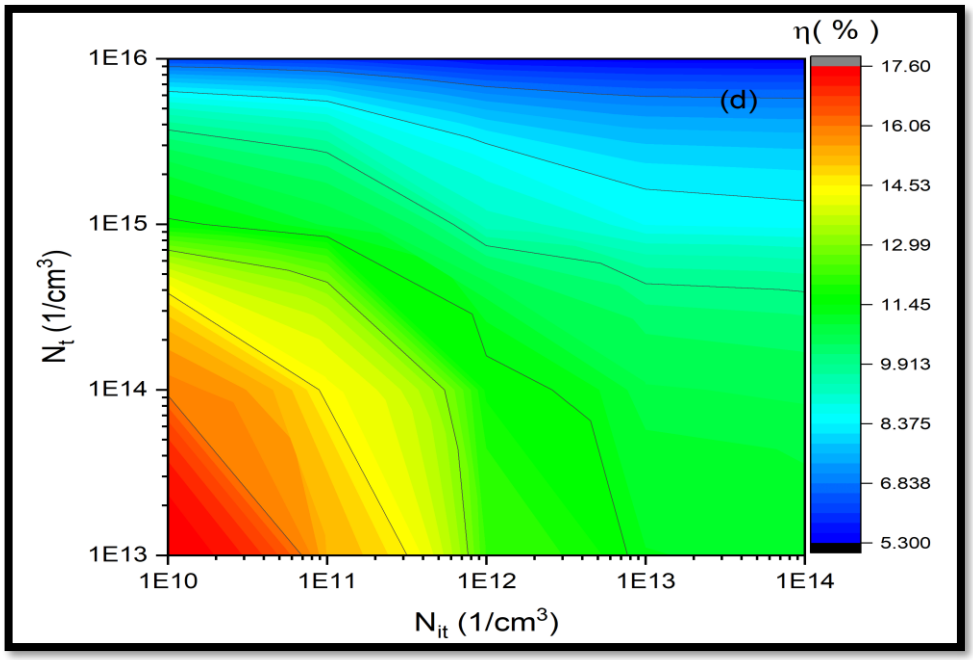

(d)

Fig. (6) The effect of the density concentration of defects in the matrix along with interfacial

defects on the (a) voc (b) jsc (c) F.F (d) eta

In contrast, alterations in interface defect density yield more significant variations in Voc, J_{SC}, FF, and η. For instance, when the bulk defect density is held constant at 10^{16} cm^{-3}, changes in interface defect density lead to notable shifts in Voc, J_{SC}, FF, and η. Specifically, V_{OC} diminishes from 0.666 to 0.664 V, J_{SC} decreases from 27.61 to 22.59 mA/cm^2, FF improves from 41.37% to 52.62, and η declines from 6.239 % to 5.35 %.

Quantitative efficiency, as depicted in Figure (7a), exhibits minimal susceptibility to changes in bulk defect density, while quantum efficiency (Figure 7b) is significantly impacted by alterations in interface defect density. These findings underscore the intricate interplay between bulk and interface defects and their profound effects on solar cell performance, highlighting the importance of defect engineering strategies for optimizing device efficiency and reliability.

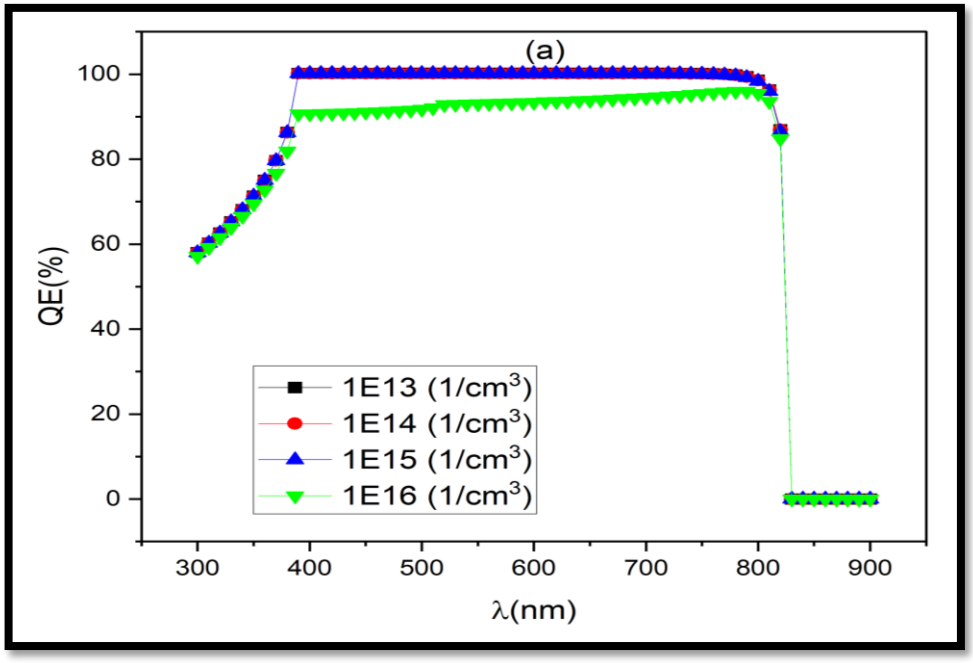

(a)

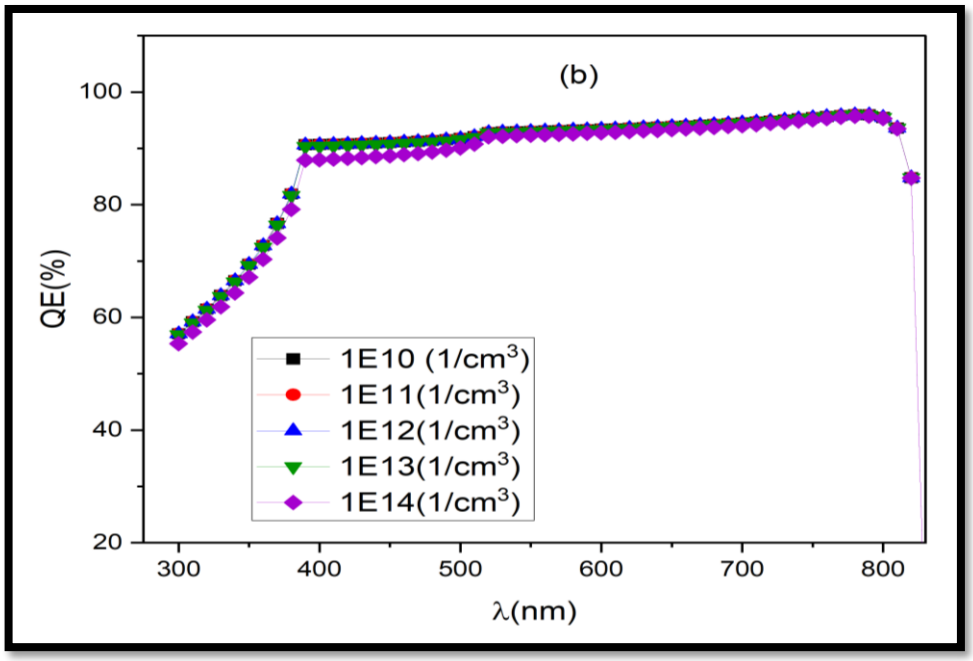

(b)

Fig. (7) (a) Quantitative efficiency with changes in bulk defects (b) Quantitative efficiency with changes in interfacial defects

4. Conclusion

This paper delves into investigating the impact of bulk defects within the CuO absorber layer on solar cell performance using SCAPS-1D. Our analysis revealed compelling insights into the intricate relationship between defect density, absorber layer thickness, and key solar cell parameters. We observed a consistent decrease in fill factor (FF), open-circuit voltage (V_{OC}), short-circuit current (J_{SC}), and overall efficiency (η) as defect levels approached mid-gap values. This underscores the detrimental effect of bulk defects on solar cell performance.

On the other hand, increasing the thickness of the absorber layer led to big improvements in Jsc, VOC, FF, and overall efficiency. This shows how important it is to find the best layer dimensions to make a device work better. Remarkably, our findings indicate that solar cell performance remains relatively stable when defect densities in the CuO layer are below 10^{14} cm-^{3}. However, exceeding this threshold resulted in a significant degradation of all cell output parameters, underscoring the critical importance of defect management in solar cell design.

In conclusion, this study underscores the necessity for meticulous defect engineering strategies to mitigate adverse effects and optimize solar cell performance, paving the way for the development of more efficient and reliable photovoltaic devices.

References

[1] A. J. C. O. i. G. Zakutayev and S. Chemistry, "Brief review of emerging photovoltaic

absorbers," vol. 4, pp. 8-15, 2017.
[2] Y. Shi, C. Sturm, and H. J. J. o. S. S. C. Kleinke, "Chalcogenides as thermoelectric materials," vol. 270, pp. 273-279, 2019.
[3] P. Bonnick et al., "Insights into Mg2+ intercalation in a zero-strain material: thiospinel Mg x Zr2S4," vol. 30, no. 14, pp. 4683-4693, 2018.
[4] K. Kaup et al., "Correlation of Structure and Fast Ion Conductivity in the Solid Solution Series Li1+ 2 x Zn1–x PS4," vol. 30, no. 3, pp. 592-596, 2018.
[5] Z. Zhang et al., "Na 11 Sn 2 PS 12: a new solid state sodium superionic conductor," vol. 11, no. 1, pp. 87-93, 2018.
[6] S. M. Kwon et al., "High-performance and scalable metal-chalcogenide semiconductors and devices via chalco-gel routes," vol. 4, no. 4, p. eaap9104, 2018.
[7] D. J. Milliron, D. B. Mitzi, M. Copel, and C. E. J. C. o. m. Murray, "Solution-processed metal chalcogenide films for p-type transistors," vol. 18, no. 3, pp. 587-590, 2006.
[8] B. J. Eggleton, B. Luther-Davies, and K. J. N. p. Richardson, "Chalcogenide photonics," vol. 5, no. 3, pp. 141-148, 2011.
[9] S. Hudgens and B. J. M. b. Johnson, "Overview of phase-change chalcogenide nonvolatile memory technology," vol. 29, no. 11, pp. 829-832, 2004.
[10] M. Rahman, M. Salleh, I. Talib, and M. J. J. o. p. s. Yahaya, "Effect of ionic conductivity of a PVC–LiClO4 based solid polymeric electrolyte on the performance of solar cells of ITO/TiO2/PVC–LiClO4/graphite," vol. 133, no. 2, pp. 293-297, 2004.
[11] A. R. Zainun, S. Tomoya, U. M. Noor, M. Rusop, and I. J. M. L. Masaya, "New approach for generating Cu2O/TiO2 composite films for solar cell applications," vol. 66, no. 1, pp. 254-256, 2012.
[12] J. Arana, A. P. Alonso, J. D. Rodríguez, J. H. Melián, O. G. Díaz, and J. P. J. A. C. B. E. Peña, "Comparative study of MTBE photocatalytic degradation with TiO2 and Cu-TiO2," vol. 78, no. 3-4, pp. 355-363, 2008.
[13] K. Chiang, R. Amal, and T. J. A. i. E. R. Tran, "Photocatalytic degradation of cyanide using titanium dioxide modified with copper oxide," vol. 6, no. 4, pp. 471-485, 2002.
[14] H. Irie et al., "Visible light-sensitive Cu (II)-grafted TiO2 photocatalysts: activities and X-ray absorption fine structure analyses," vol. 113, no. 24, pp. 10761-10766, 2009.
[15] M. Ichimura and Y. J. M. S. i. S. P. Kato, "Fabrication of TiO2/Cu2O heterojunction solar cells by electrophoretic deposition and electrodeposition," vol. 16, no. 6, pp. 1538-1541, 2013.
[16] R. T. J. M. S. Tung and E. R. Reports, "Recent advances in Schottky barrier concepts," vol. 35, no. 1-3, pp. 1-138, 2001.
[17] S. Hussain et al., "Cu2O/TiO2 nanoporous thin-film heterojunctions: Fabrication and electrical characterization," vol. 25, pp. 181-185, 2014.
[18] S. Hussain et al., "Fabrication and photovoltaic characteristics of Cu2O/TiO2 thin film heterojunction solar cell," vol. 522, pp. 430-434, 2012.
[19] Y. H. Khattak et al., "Effect of CZTSe BSF and minority carrier life time on the efficiency enhancement of CZTS kesterite solar cell," vol. 18, no. 6, pp. 633-641, 2018.
[20] F. A. Jhuma, M. Z. Shaily, M. J. J. M. f. R. Rashid, and S. Energy, "Towards high-efficiency CZTS solar cell through buffer layer optimization," vol. 8, pp. 1-7, 2019.
[21] F. H. Oraibi and F. A. J. J. o. K.-P. AL-Tememe, "Theoretical Study of the effect of impurity concentrations on the efficiency of the single crystal silicon solar cell," vol. 4, no. 1, 2012.
[22] H. Guo, Y. Li, X. Guo, N. Yuan, and J. J. P. B. C. M. Ding, "Effect of silicon doping on electrical and optical properties of stoichiometric Cu2ZnSnS4 solar cells," vol. 531, pp. 9-15, 2018.
[23] K. Mukhopadhyay, P. F. H. Inbaraj, and J. J. J. M. R. I. Prince, "Thickness optimization of CdS/ZnO hybrid buffer layer in CZTSe thin film solar cells using SCAPS simulation

program," 2018.
[24] F. Baig, "Numerical analysis for efficiency enhancement of thin film solar cells," Universitat Politècnica de València, 2019.
[25] A. Spies, J. Reinhardt, M. List, B. Zimmermann, and U. J. E. P. i. O. P. Würfel, "Impact of charge carrier mobility and electrode selectivity on the performance of organic solar cells," pp. 401-418, 2017.
[26] F. Baig et al., "Numerical analysis of a novel FTO/n-MAPbI3/p-MAPbI3/p-MAPbBr3 organic–inorganic lead halide perovskite solar cell," vol. 13, no. 9, pp. 1320-1327, 2018.